Mon. Not. R. Astron. Soc. **353,** 647–653 (2004) doi:10.1111/j.1365-2966.2004.08099.x

Early afterglow emission from a reverse shock as a diagnostic tool for gamma-ray burst outflows

Ehud Nakar[1,2⋆] and Tsvi Piran[1]

[1]*Racah Institute for Physics, The Hebrew University, Jerusalem 91904, Israel*
[2]*Institut d'Astrophysique de Paris, 75014 Paris, France*

Accepted 2004 June 2. Received 2004 June 2; in original form 2004 April 20

ABSTRACT

The gamma-ray burst–afterglow transition is one of the most interesting and least studied gamma-ray burst phases. During this phase, the relativistic ejecta begins interacting with the surrounding matter. A strong short-lived reverse shock propagates into the ejecta (provided that it is baryonic) while the forward shock begins to shape the surrounding matter into a Blandford–McKee profile. We suggest a parametrization of the early afterglow light curve and we calculate (analytically and numerically) the observed parameters that result from a reverse shock emission (in an interstellar medium environment). We present a new fingerprint of the reverse shock emission that is added to the well-known t^{-2} optical decay. Observation of this signature would indicate that the reverse shock dominates the emission during the early afterglow. The existence of a reverse shock will in turn imply that the relativistic ejecta contains a significant baryonic component. This signature would also imply that the surrounding medium is an interstellar medium. We further show the following. (i) The reverse shock optical flash depends strongly on initial conditions of the relativistic ejecta. (ii) Previous calculations have generally overestimated the strength of this optical flash. (iii) If the reverse shock dominates the optical flash, then detailed observations of the early afterglow light curve would possibly enable us to determine the initial physical conditions within the relativistic ejecta and specifically to estimate its Lorentz factor and its width.

Key words: hydrodynamics – shock waves – gamma-rays: bursts.

1 INTRODUCTION

According to the internal–external shock model (Piran & Sari 1998), the prompt gamma-ray burst (GRB) is produced by internal shocks within a relativistic flow while the afterglow is produced by external shocks between this flow and the surrounding matter. The early afterglow appears during the transition from the prompt gamma-ray emission to the afterglow. During this transition, the relativistic flow, ejected by the source, interacts directly with the circumburst medium. This interaction can be used to pin down the nature of the relativistic flow (baryonic or Poynting flux). In a baryonic flow, the reverse shock (RS) that propagates into the ejecta produces both optical and radio emission. With Poynting flux we expect only the higher energy forward shock (FS) emission. While other sources of early optical and radio emission may exist also in Poynting flux flow, we show here that the RS emission has a very robust optical and radio observable signature that is very unlikely to be imitated by other phenomena. If the flow is found to be baryonic, then the early afterglow signal could serve as a diagnostic tool for the properties of the ejecta. This, in turn, would shed light on the nature of the inner engine that powers the GRB.

Numerous authors (Mészáros & Rees 1997; Sari & Piran 1999a; Kobayashi 2000; Sari & Mészáros 2000; Soderberg & Ramirez-Ruiz 2003a; Zhang, Kobayashi & Mészáros 2003) have considered the emission from the RS. Strong optical flashes in a rough agreement with the RS predictions (Mészáros & Rees 1999; Sari & Piran 1999b; Wang, Dai & Lu 2000; Fan et al. 2002; Fox et al. 2003a; Kumar & Panaitescu 2003; Soderberg & Ramirez-Ruiz 2003b; Weidong et al. 2003) were observed in two bursts (GRBs 990123 and 021211). In the first, the RS predicted radio flare was observed as well (Kulkarni et al. 1999; Sari & Piran 1999b). On the other hand, the early (the first 10 min) optical emission observed in two other bursts (GRBs 021004 and 030418; Fox et al. 2003b; Rykoff et al. 2004) did not agree with the simple predictions of an RS emission (see, however, Kobayashi & Zhang 2003a). Furthermore, upper limits of ∼15 mag on the prompt optical flux of several bursts (Williams, Park & Porrata 1999; Rykoff & Smith 2002; Klotz et al. 2003; Torii 2003a,b) have led to the so-called 'optical flash problem': lack of bright optical flashes (corresponding to RS emission) in many bursts.

Swift is expected to provide a large number of deep (∼20 mag) early (∼1 min) optical observations. We provide here detailed

⋆E-mail: udini@phys.huji.ac.il

predictions of the RS emission of a baryonic flow that interacts with a constant density circumburst medium – such as an interstellar medium (ISM). These predictions can be confronted with the upcoming observations. We show that when the early afterglow is found to be dominated by such RS emission (by passing the observational tests) then the observations enable us to determine the initial physical properties of the relativistic outflow and to constrain the microscopic parameters in the emitting region. We also show that the peak flux depends sensitively on the strength of the RS. It can vary over more than five optical magnitudes between mildly relativistic and ultrarelativistic shocks. Furthermore, previous calculations have generally overestimated the peak flux of the mildly relativistic RS by up to seven optical magnitudes. In fact, the FS emission may even dominate over the RS emission at early times. Altogether these results suggest a solution to the 'optical flash problem'. The calculated radio light curve shows that the radio flare lasts long after the optical flash. We find that, in the generic case, in addition to the typical decay of the optical flash (Sari & Piran 1999a), the flash to flare time ratio and intensity ratio provide another new test that the emission results from an RS.

Other mechanisms apart from the RS in an ISM environment can produce an optical flash. A few examples are internal shocks (Mészáros & Rees 1997), a pair avalanche (Thompson & Madau 2000; Meszaros, Ramirez-Ruiz & Rees 2001; Beloborodov 2002), RS produced in a wind environment (Chevalier & Li 2000; Kobayashi & Zhang 2003b; Wu et al. 2003; Kobayashi, Mészáros & Zhang 2004) and even the FS as we discuss here. While these mechanisms might be able to produce a bright early optical flash, they are not expected to produce the combination of the early optical and radio emission that we show here to arise from an RS in an ISM environment.[1] Thus, observing this signature in many bursts in the future will solve further open questions than just the flow's constitution (baryonic versus Poynting flux). It will also reveal the circumburst density profile and determine the dominant mechanism that contributes to the optical flash. In a separate paper (Nakar & Piran 2004) we apply the tests and the diagnostic tools presented here to GRB 990123. We find that its early afterglow emission is remarkably consistent with our predictions of the RS emission, suggesting strongly that at least in this case the early afterglow is produced by a baryonic flow propagating into an ISM.

The structure of the paper is somewhat unusual. The RS emission in the most general case presents a large and complex diversity, but the generic behaviour is rather simple. Therefore, we begin in Section 2 with a summary of the generic optical and radio observables. We demonstrate how to use them in order to confirm that the emission results from an RS and, in this case, to determine the physical properties of the relativistic outflow. Later, we describe the general analytical theory (Section 3) and the numerical simulations (Section 4).

2 GENERIC EARLY AFTERGLOW LIGHT CURVE

Consider a homogeneous[2] cold baryonic shell expanding relativistically into a homogeneous cold ISM. The problem is well defined by the shell's (isotropic equivalent) energy E, width Δ, initial Lorentz factor $\Gamma_{\rm o}$ and the ISM density n. As the ejecta shovels the ISM, a FS and an RS are produced. The nature of the RS is determined by the dimensionless parameter $\xi \equiv (l/\Delta)^{1/2}\Gamma_{\rm o}^{-4/3}$ (Sari & Piran 1995, hereafter SP95), where $l \equiv [3E/(4\pi\, nm_{\rm p}c^2)]^{1/3}$. If $\xi \ll 1$ the RS is relativistic and most of the shell's bulk motion energy is dissipated in a single shock crossing of the shell, which occur at a radius $R_\Delta \approx l^{3/4}\Delta^{1/4}$ (SP95). For $\xi \gg 1$ the RS is Newtonian and many crossings are required to dissipate a significant fraction of the energy. In the generic case $\xi \lesssim 1$. In this case after the RS crosses the ejecta once, the circumburst gas, shocked by the FS, forms a Blandford–Mckee profile and the original ejecta expands and cools down at the tail of this profile (Kobayashi & Sari 2000, hereafter KS00). Therefore, the hydrodynamical (and the radiative) evolution is separated into two phases: during the RS and after the RS. The emission from the separation point reaches the observer simultaneously with a photon emitted on the line of sight from the rear end of the shell at R_Δ:

$$t_0 = \left(\frac{\Delta}{c} + \frac{R_\Delta}{2c\Gamma_{\rm o}^2}\right)(1+z) = \frac{\Delta}{c}\left(1 + 0.5\mathcal{N}_t\xi^{3/2}\right)(1+z). \qquad (1)$$

Here, c is the light speed, z is the redshift and $\mathcal{N}_t = 1.4$. Here and throughout the paper $\mathcal{N}_x$ denotes numerical correction factors to the analytical estimates (see Section 4).

The evolution before t_0 is highly sensitive to the initial profile of the shell and in particular to the value of ξ. Thus the observables before and at t_0 depend strongly on the initial properties of the shell, and as such can be used as a diagnostic tool of these properties. On the other hand, the RS that crosses the shell erases, to a large extend, the initial shell profile. Moreover, the evolution during the expanding and cooling phase depends only weakly on ξ (KS00). Therefore, the behaviour after t_0 is insensitive to the initial conditions and as such it provides a very unique and easily identified signature of an RS emission.

The general behaviour of a basic RS (i.e. with no complications as refreshed shocks during the RS, etc.) over a broad spectrum is described in Table 1. In this section we summarize only the generic behaviour of the optical and radio observables and demonstrate how to determine the physical parameters, ξ, Δ and $\Gamma_{\rm o}$, from the optical light curve. This should be used with care as a non-generic behaviour is always a possibility.

The RS optical flash peaks at t_0. Therefore, similar to late afterglow parametrization (Beuermann et al. 1999), we suggest to parametrize the RS optical emission as

$$F^r_{\nu,\rm opt}(t) = F^r_0\left[\frac{1}{2}\left(\frac{t}{t_0}\right)^{-s\alpha_1} + \frac{1}{2}\left(\frac{t}{t_0}\right)^{-s\alpha_2}\right]^{-(1/s)}, \qquad (2)$$

where $\alpha_1 > 0$ and $\alpha_2 < 0$ are the power-law indices of a broken power law that peaks at[3] $\approx F^r_{\nu,\rm opt}(t_0) = F^r_0$. s determines the sharpness of the peak. The optical frequency, $\nu_{\rm opt}$, is expected to satisfy $\nu^r_{\rm a}, \nu^r_{\rm m} < \nu_{\rm opt} < \nu^r_{\rm c}$ where $\nu^r_{\rm a}$, $\nu^r_{\rm m}$ and $\nu^r_{\rm c}$ are the self-absorbtion, synchrotron and cooling frequencies in the RS, respectively. In this case (Sari & Piran 1999a)

$$\alpha_2 \approx -2. \qquad (3)$$

The decay slope, α_2, as a post-t_0 observable, is very robust. KS00 show numerically that $\alpha_2 \approx -2$ for various values of ξ and p and

[1] For example, in the pair avalanche process the optical flash results from a pair enriched FS and this emission is becoming harder with time (Beloborodov 2002), in contrast to the RS emission. Thus, no correlated radio flare is expected.

[2] The limits of the results presented in this section when the shell is inhomogeneous are discussed in Section 4.

[3] For $s \gtrsim 1$ the peak of equation (2) is obtained at $\approx t_0$ and its value is $\approx F^r_0$. Numerical simulations show that in the case analysed here indeed $s \gtrsim 1$ (see Section 4). Thus, t_0 and F^r_0, which are found according to the best fit of equation (2), can be taken, for any practical purpose, directly from the observations as the time and the flux of optical peak.

Table 1. The break frequencies and maximal flux densities. ϵ_e and ϵ_B are the fraction of the internal energy in relativistic electrons and the magnetic field, respectively, p is the electron spectral index, and D is the proper distance to the burst. $\overline{\epsilon}_e \equiv 30\epsilon_e(p-2)/(p-1)$, $b_\xi \equiv (1+\mathcal{N}_t 0.5\xi^{3/2})$, $h_a \equiv a^2+1.5a+1$ and $\overline{A}^x_x(\xi) \equiv A^x_x(\xi)/A^x_x(1)$. Using the table, $F_\nu(\nu)$ is found according the maximal flux, $F_{\nu,\max}$, the values of the break frequencies and the spectral power-law indices between them. All these vary between the different cases, where at each case $F_{\nu,\max}$ is at a different break frequency. $\nu_m < \nu_a < \nu_c$ (generic case): $F_{\nu,\max}(\nu=\nu_a) = F_{\nu,b}(\nu_a/\nu_m)^{(1-p)/2}$; power-law indices, $2 < \nu_m < 2.5 < \nu_a < (1-p)/2 < \nu_c < -p/2$. $\nu_a < \nu_m < \nu_c$: $F_{\nu,\max}(\nu=\nu_m) = F_{\nu,b}$; power-law indices, $2 < \nu_a < 1/3 < \nu_m < (1-p)/2 < \nu_c < -p/2$. $\nu_a < \nu_c < \nu_m$: $F_{\nu,\max}(\nu=\nu_c) = F_{\nu,b}$; power-law indices, $2 < \nu_a < 1/3 < \nu_c < -1/2 < \nu_m < -p/2$. Column 2 gives the values at $t = t_0$. Column 3 gives the dependence at $t \leqslant t_0$ on ξ. In column 4, the evolution at $t < t_0$ can be found using this column and equation (14) (see Section 3). Column 5 gives the approximated power-law indices at $t > t_0$; these values are uncertain by at least ± 0.05–0.1 (see KS00). The values are calculated using the hydrodynamics of equations (12) and (16) ($t < t_0$) and KS00 ($t > t_0$), and the radiation calculations described in Sari, Piran & Narayan (1998), Granot, Sari & Piran (1999) and Granot & Sari (2001).

	Value at $t = t_0$	$A^x_x(\xi)$	at $t < t_0$	$t > t_0$
ν^r_m	$2\times10^{11}\,\mathrm{Hz}(1+z)^{-(1/4)}\overline{\epsilon}_e^2\epsilon_{B-2}^{1/2}n^{1/4}E_{52}^{1/4}t_{0,2}^{-(3/4)}\overline{A}^r_{\nu,m}(\xi)$	$a^8h_a^{-2}\xi^{-7.5}b_\xi^{3/4}$	$\propto f^2a^8h_a^{-2}$	-1.5
ν^{ra}_c	$1\times10^{17}\,\mathrm{Hz}(1+z)^{-1/2}\epsilon_{B-2}^{-3/2}n^{-1}E_{52}^{-1/2}t_{0,2}^{-1/2}\overline{A}^r_{\nu,c}(\xi)$	$a^{-4}\xi^3b_\xi^{-3/2}$	$\propto f^{-2}a^{-4}b_\xi^{-2}$	
ν^{rb}_a	$(5p+2)10^{12}\,\mathrm{Hz}(1+z)^{-(2/5)}\overline{\epsilon}_e^{-1}\epsilon_{B-2}^{1/5}n^{2/5}E_{52}^{2/5}t_{0,2}^{-(3/5)}\overline{A}^r_{\nu,a}(\xi)$	$a^{-8/5}h_a\,\xi^{12/5}b_\xi^{3/5}$	$\propto f^{-1}a^{-8/5}h_a$	-0.55
ν^{rc}_a	$(p-0.8)10^{13}\,\mathrm{Hz}\left[(1+z)^{-(p+6/8)}\overline{\epsilon}_e^{p-1}\epsilon_{B-2}^{(p+2)/4}(nE_{52})^{(p+6)/8}t_{0,2}^{-(3p+10/8)}a^{4p}h_a^{1-p}\xi^{(6-15p)/4}b_\xi^{(3p+10/8)}\right]^{2/(p+4)}$		$\propto\left[\left(\frac{f}{h_a}\right)^{p-1}a^{4p}\right]^{2/(p+4)}$	-1
$F^r_{\nu,b}$	$250\,\mathrm{mJy}(1+z)^{-(5/8)}\epsilon_{B-2}^{1/2}n^{3/8}E_{52}^{9/8}t_{0,2}^{-3/8}D_{28}^{-2}\overline{A}^r_{F,b}(\xi)$	$a^2\xi^{-3/4}b_\xi^{3/8}$	$\propto fa^2$	-0.95
ν^f_m	$1\times10^{16}\,\mathrm{Hz}(1+z)^{1/2}\overline{\epsilon}_e^2\epsilon_{B-2}^{1/2}E_{52}^{1/2}t_{0,2}^{-3/2}\overline{A}^f_{\nu,m}(\xi)$	$a^4\xi^{-3}b_\xi^{3/2}$	$\propto a^4$	-1.5
ν^{fb}_a	$3\,\mathrm{GHz}(1+z)^{-1}\overline{\epsilon}_e^{-1}\epsilon_{B-2}^{1/5}n^{3/5}E_{52}^{1/5}\overline{A}^f_{\nu,a}(\xi)$	$a^{2/5}\xi^{-3/10}$	$\propto f^{3/10}a^{2/5}$	0
ν^{fd}_a	$0.6\,\mathrm{GHz}(1+z)^{-(1/2)}\epsilon_{B-2}^{6/5}n^{11/10}E_{52}^{7/10}t_{0,2}^{-1/2}\overline{A}^f_{\nu,a}(\xi)$	$a^{22/5}\xi^{-(33/10)}b_\xi^{3/2}$	$\propto f^{13/10}a^{22/5}b_\xi$	-0.5
$F^f_{\nu,b}$	$1.5\,\mathrm{mJy}(1+z)^{-1}\epsilon_{B-2}^{1/2}n^{1/2}E_{52}D_{28}^{-2}\overline{A}^f_{F,b}(\xi)$	$a^2\xi^{-3/2}$	$\propto f^{3/2}a^2$	0

Notes. [a] $\nu^f_c = \nu^r_c$ at $t < t_0$. [b] $\nu_a < \nu_m < \nu_c$. [c] $\nu_m < \nu_a < \nu_c$. [d] $\nu_a < \nu_c < \nu_m$.

thus it is a signature of a generic RS emission. On the other hand, α_1 is most sensitive to ξ. When $\xi \ll 1$, $\alpha_1 \approx 0.5$ and as ξ increases so does α_1. For $0.05 < \xi < 5$ it can be well approximated as (see Fig. 2a)

$$\alpha_1 \approx \mathcal{N}_{\alpha,1}\left[0.5 + \frac{p}{2}(\xi - 0.07\xi^2)\right], \quad (4)$$

where p is the power-law index of the electron energy distribution, and $\mathcal{N}_{\alpha,1} = 1.2$. Thus, a measurement of α_1 can determine the value of ξ (up to the uncertainty in the value of p). Once ξ is known, equation (1) is solved for Δ. Having ξ and Δ we can find Γ_o using

$$\Gamma_o = 188\xi^{-3/4}\Delta_{12}^{-3/8}(E_{52}/n)^{1/8}, \quad (5)$$

where we denote by Q_x the value of the quantity Q in units of 10^x (c.g.s). Note that when $\xi \ll 1$ both equations (1) and (4) are insensitive to ξ and only a lower limit of Γ_o can be found. Γ_o depends very weakly on the ratio E/n. Finally, we find numerically that the sharpness parameter s depends strongly on the initial profile of the shell, but not on ξ. The larger the initial Lorentz factor dispersion ($\delta\Gamma_o = \Gamma_{o,\max}/\Gamma_{o,\min}$) is, the smaller s is (wider peak). A homogeneous shell ($\delta\Gamma_o = 1$) results in a very sharp peak, $s \approx 10$, while mild dispersion of $\delta\Gamma_o = 2$ may be sufficient to reduce s to ≈ 1.

It is remarkable that these initial parameters can be determined without using F_0^r, and thus with no dependence on the poorly known internal parameters, ϵ_e and ϵ_B. The value of F_0^r can be used to constrain these parameters:

$$\begin{aligned} F_0^r &= 0.6\,\mathrm{mJy}\mathcal{N}_F(1+z)^{-(4+p/8)}1.5^{2.5-p} \\ &\times\left[\frac{3(p-2)}{p-1}\right]^{p-1}\epsilon_{e-1}^{p-1}\epsilon_{B-2}^{(p+1/4)}n^{(p+2/8)} \\ &\times E_{52}^{1+(p/8)}t_{0,2}^{-(3p/8)}D_{28}^{-2}A_{F,0}^r(\xi). \end{aligned} \quad (6)$$

Here, the numerical correction factor is $\mathcal{N}_F \approx 1/5$ and all the parameters and notations are as in Table 1. The function $A_{F,0}^r(\xi)$ is approximated in the range of $0.1 < \xi < 2.5$ by

$$A_{F,0}^r(\xi) \approx 180\xi^{0.65}\left(6\times10^{-4}\xi^{-2.6}\right)^{(p-1/2)}. \quad (7)$$

The exact value of $A_{F,0}^r$ is given in equation (13), and must be used when ξ is outside the range above. F_0^r depends strongly on ξ and it varies by two orders of magnitude within the range most relevant for GRBs ($0.1 < \xi < 3$). The relativistic and the Newtonian approximations (Fig. 1b) overestimate F_0^r. Specifically, the commonly used Newtonian approximation overestimates $F_0^r(\xi = 1)$ by a factor of 200. The numerical correction factor, $\mathcal{N}_F$, adds another factor of 5.

The radio emission continues to rise after t_0 and it peaks at a later time, t_*, when $\nu_{radio} = \nu_a^r$. This happens during the 'cooling' phase of the shocked shell material. Therefore, the radio behaviour both before and after t_* is a robust feature (i.e. does not depend on the initial conditions). The light curve depends only on the relations between ν_m^r, ν_a^r and ν_{radio} and the only remaining influence of the initial conditions is via the values of the break frequencies at t_0. Over a wide range of ξ values $\nu_m^r(t_0) < \nu_a^r(t_0) \approx 10^{12-13}$ Hz.[4] In this case, the radio flux at $t > t_0$ can be also characterized by the

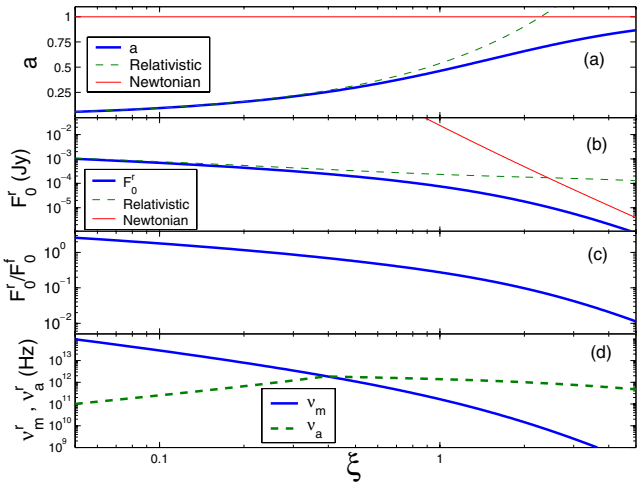

Figure 1. The parameter, a, and various break frequencies and flux densities as functions of ξ. (a) The parameter a according to equation (11) (thick line), and its relativistic (dashed line) and Newtonian (thin line) approximations. (b) F_0^r according to equations (6) and (13) when a is calculated according to equation (11) (thick line), and when the relativistic (dashed line) or Newtonian (thin line) approximation of a is taken. The physical parameters considered here are similar to these considered in panel d. (c) The ratio between the RS peak flux and the FS flux at the same time. ϵ_e and ϵ_B are assumed to be similar in the RS and the FS. (d) The synchrotron (solid line) and the self-absorbtion (dashed line) frequencies of the RS emission at t_0. The parameters considered here are $E_{52} = 1$, $\epsilon_e = 0.1$, $\epsilon_B = 0.01$, $n = 1$, $p = 2.5$, $t_0 = 100$ s and $z = 1$ ($D_{28} = 1$).

parametrization of equation (2) with (see Table 1)[5]

$$\begin{aligned} &\alpha_{r,1} \approx 1.25 \qquad \alpha_{r,2} \approx -2 \\ &\frac{t_*}{t_0} = \frac{\nu_a^r(t_0)}{\nu_{radio}} \\ &\frac{F_*}{F_0} = \left[\frac{\nu_a^r(t_0)}{\nu_{opt}}\right]^{-(p-1/2)}\left(\frac{\nu_{radio}}{\nu_a^r(t_0)}\right)^{1.3}. \end{aligned} \quad (8)$$

Equation (8) predicts a relation between the optical and radio emission of the RS. It provides both an estimate of $\nu_a^r(t_0)$ and a test that the emission results from an RS:

$$\frac{F_*}{F_0}\left(\frac{t_*}{t_0}\right)^{(p-1/2)+1.3} = \left(\frac{\nu_{opt}}{\nu_{radio}}\right)^{(p-1/2)} \sim 1000. \quad (9)$$

Note that this value can be larger or smaller by a factor of ~ 3 (for a given p), because of the uncertainty in the post-RS dynamics (KS00). Together with the optical decay signature, equations (8) and (9) provide a unique imprint of a baryonic RS. The determination of $\nu_a^r(t_0)$ (and maybe even $\nu_m^r(t_0)$) provide additional constraints on ϵ_e and ϵ_B.

The early afterglow behaviour described above is relevant only when the RS is produced by interaction with ISM-like densities or lower ($n \lesssim 100$ cm^{-3}). This condition is not satisfied if the circumburst medium is the wind of a massive star. For any reasonable parameters of such a wind, the external density during the crossing of the RS is a few orders of magnitude larger than that of a typical ISM. This brings the cooling frequency well below the optical bands (Chevalier & Li 2000) and possibly the self-absorbtion frequency

[4] A different case from the generic one (i.e. different relation between ν_m^r, ν_a^r and ν_{radio}) is more likely here than in the optical emission, especially when the RS is ultrarelativistic.

[5] As long as $\nu_{radio} < \nu_m^r$, $\alpha_r \approx 0.5$. Observing the transition time to $\alpha_{r,1} \approx 1.25$ determines $\nu_m^r(t_0)$. The early behaviour at $t < t_0$ can be found from Table 1.

above the optical band (Kobayashi et al. 2004). This change of the frequencies sequence changes also the resulting behaviour of the optical light curve (e.g. the value of α_2). Therefore, observing an early afterglow that shows the RS emission signature described above implies also that the density of the external medium is ISM-like.

3 THEORY

The nature of the RS is determined by the dimensionless parameter ξ, which in turn determines the ratio, a, of the Lorentz factor of the shocked matter (in the explosion rest frame), γ_r, to Γ_o:

$$a \equiv \gamma_r/\Gamma_o. \tag{10}$$

a can be derived directly from the relativistic jump conditions (SP95). It satisfies[6]

$$(12/\xi^3 - 1)a^4 + 0.5a^3 + a^2 + 0.5a - 1 = 0. \tag{11}$$

In the relativistic regime $a \approx a_R = 12^{-1/4}\xi^{3/4}$, while in the Newtonian regime $a \approx a_N = 1$. Both approximations overestimate a in the intermediate regime and the deficiency is largest when $\xi \approx 1$ (Fig. 1a). For $\xi \lesssim$ a few, the RS emission peaks when the RS reaches the back of the shell. At this stage the pressure, p_r, and the density, n_r, in the shocked shell as measured in the shocked fluid rest frame, are

$$p_r = \frac{4}{3}a^2\Gamma_o^2 n m_p c^2; \qquad n_r = \xi^3 n \Gamma_o^2 [2(a + 1/a)/3 + 1]. \tag{12}$$

Assuming a homogeneous initial shell and homogeneous conditions within the shocked region,[7] these hydrodynamical conditions determine ν_a^r, ν_m^r, ν_c^r and the peak flux $F_{\nu,\max}^r$ at $t = t_0$. These values appear in Table 1 and can be used to estimate the radio and the optical emission at t_0. Using these values we derive the optical emission, equation (6) and the exact value of $A_{F,0}^r(\xi)$:

$$A_{F,0}^r(\xi) = 770a^{4p-2}(a^2 + 1.5a + 1)^{1-p}\xi^{3-3.75p} \times(1 + 0.5\mathcal{N}_t\xi^{3/2})^{3p/8}. \tag{13}$$

Next we consider the evolution at $t < t_0$. The flux at $t < t_0$ can be determined by parametrizing all the quantities according to the fraction, f, of the shell that the RS has crossed: $\Delta(f)$ and $E(f) \propto f$ while n is constant. This implies $\xi(f) \propto f^{-1/3}$ and $R(f) \propto f^{1/2}$. The observer time

$$t(f) \propto f\left[1 + 0.5\mathcal{N}_t\xi(f)^{3/2}\right] \tag{14}$$

and the optical flux (for ν_a^r, $\nu_m < \nu_{opt} < \nu_c^r$; see Table 1)

$$F_{\nu,opt}^r(f) \propto f^p a^{4p-2}(a^2 + 1.5a + 1)^{1-p}, \tag{15}$$

combine to yield α_1. In the relativistic regime ($a \propto \xi^{3/4} \propto f^{-1/4}$) $t \propto f$ and $F_0 \propto f^{1/2}$, hence $\alpha_1 = 0.5$. When ξ increases, the logarithmic time derivative, $\mathrm{d}\log(F_{\nu,opt}^r)/\mathrm{d}\log(t)$, varies with time, and its value at $t < t_0$ depends strongly on ξ. The description of the light curve as a power law with an index α_1 is only an approximation. We estimate α_1 as the mean value of $\mathrm{dlog}(F_{\nu,opt}^r)/\mathrm{dlog}(t)$ during $t_0/2 < t < t_0$, and compare it to the standard deviation in this time range (Fig. 2a). The small deviation compared to the mean value justifies the power-law approximation.

The evolution at $t > t_0$ is dictated by the post-RS hydrodynamics.

[6] For a relativistic adiabatic constant – 4/3. Our results do not change significantly if the adiabatic constant varies smoothly between 4/3 when $\xi \ll 1$ to 5/3 when $\xi \gg 1$.

[7] These assumptions are relaxed in the numerical simulations.

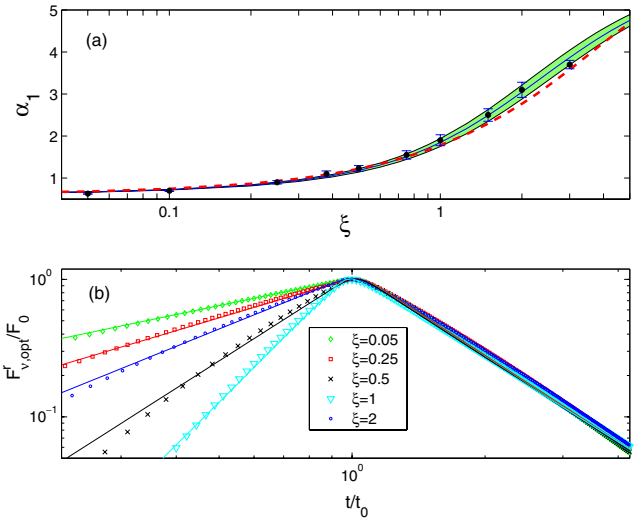

Figure 2. Results of detailed hydro+synchrotron numerical simulations. (a) $\alpha_1(\xi)$ as estimated by the mean value of $\mathrm{d}\log(F_{\nu,opt}^r)/\mathrm{d}\log(t)$ at $t_0/2 < t < t_0$, according to equations (14) and (15) (thin line), according to equation (4) (dashed line) and according to the numerical simulations (dots). The standard deviation of $\mathrm{d}\log(F_{\nu,opt}^r)/\mathrm{d}\log(t)$ at $t_0/2 < t < t_0$ is depicted by the shaded area (equations 14 and 15) and the error bars (numerical simulations). (b) Five numerical (normalized) optical light curves with various ξ values, and their best fits according to equation (2) (see Section 4).

This hydrodynamics evolution was investigated both analytically and numerically in KS00, and was found to be almost independent of ξ. We use the hydrodynamic evolution presented in KS00 to determine the optical and radio light curves.

Finally, we calculate the contribution of the FS emission. The FS hydrodynamical conditions at R_Δ are

$$\gamma_f = \gamma_r; \qquad p_f = p_r; \qquad n_f = 4a\Gamma_o n. \tag{16}$$

The corresponding spectral parameters at t_0 ($\nu_{a,m,c}^f(t_0)$ and $F_{\nu,\max}^f(t_0)$) are listed in Table 1. The FS emission, in contrast to the RS emission, depends rather weakly on ξ. Thus, the ratio between the two varies strongly with ξ. Specifically, the widely used relation $\nu_m^f/\nu_m^r = (n_r/n_f)^2$ depends strongly on ξ. For $\xi \approx 1$ it indeed equals $\approx \Gamma_o^2$. However, for $\xi = 0.1$ this ratio equals $\approx 5 \times 10^{-4}\Gamma_o^2$. Similarly, the ratio $F_{\nu,opt}^f(t_0)/F_{\nu,opt}^r(t_0)$ determines whether the RS or the FS dominates the emission. Fig. 1(c) depicts this ratio for typical parameters. With these specific parameters, and assuming similar ϵ_e and ϵ_B in both regions, the FS optical emission cannot be neglected for $\xi > 0.5$.

4 NUMERICAL SIMULATIONS AND INHOMOGENEOUS SHELLS

The analytical calculations presented above include several approximations. In order to verify the accuracy of the analytical calculations, we carried out detailed numerical simulations (Nakar & Granot, in preparation) of the early afterglow emission. We use these simulations to determine numerical correction factors, denoted $\mathcal{N}_X$, for the analytical calculations. The hydrodynamics simulations were carried out using a one-dimensional Lagrangian code that was provided to us generously by Re'em Sari and Shiho Kobayashi (KS00). The synchrotron radiation code is described in Nakar & Granot (in preparation). This code provides an accurate synchrotron light curve and spectrum, taking into account the realistic hydrodynamical

profile[8] of the emitting region, the exact heating and cooling history of the electrons and the precise photon arrival time to the observer from each radiating element.

We have carried the simulations for a range of parameters with $0.05 \leqslant \xi \leqslant 3$. Using these simulations we obtain numerical correction coefficients and determine the accuracy of the analytical estimates of t_0, F_0^r, $F_{\nu,\rm opt}^f$ and α_1. We find that when including the numerical correction factors (that range from 0.2 to 1.4), equation (1) for t_0 is accurate up to 10 per cent while equation (6) (for $F_{\nu,\rm opt}^r$) and the expression for $F_{\nu,\rm opt}^f$ are accurate up to a factor of 2. The sharpness parameter s was not considered before, and we find its value numerically. We find that if the shell is homogeneous the peak is very sharp, $s \approx 10$, regardless of the value of ξ. Fig. 2(b) depicts five numerical light curves with $0.05 \leqslant \xi \leqslant 2$, and their best fits according to equation (2). In all these fits, F_0 is within factor of 2 of equation (6), t_0 is within 10 per cent of equation (1), α_1 is within the spread of equation (4) (the shaded area in Fig. 2a), $\alpha_2 \approx -2$ and $s \approx 10$.

So far we have considered homogeneous shells. Clearly, the light curve resulting from an inhomogeneous shell would depend on the shell's profile. To investigate partially the effect of inhomogeneity, we have carried out numerical simulations of shells with linear Lorentz factor profile ($\delta\Gamma_{\rm o} = 1.6$) and a constant energy per rest-frame length interval. The value of ξ varied between 0.05 and 1 where $\Gamma_{\rm o}$ is taken as the mean value of the initial Lorentz factor. As expected in all the cases, we find $\alpha_2 \approx -2$ (which indicates that also the radio emission should be insensitive to the shell's initial profile) and a sharp decrease in s when $\xi \approx 1$ ($s \approx 1$ compared to $s \approx 10$ in the homogeneous case). F_0^r, t_0 and α_1 are similar to the values obtained in the homogeneous case (a maximal difference of a factor of 1.5 between the homogeneous and inhomogeneous cases).[9] These results make us confident that the solution we present here for homogeneous shell is generic and applicable also for inhomogeneous shells (at least as long as $\delta\Gamma_{\rm o}$ is not much greater than 1, and the Lorentz factor profile rises monotonically and regularly).

Finally we discuss briefly two caveats, which may arise naturally in a baryonic relativistic flow, and may alter the RS emission and produce a non-generic RS optical light curve. The first caveat is a slow tail of the wind with a small, but not negligible, amount of energy (compared to the total energy of the wind). Such a tail may result from the adiabatic cooling of the wind after the phase of the prompt gamma-ray emission, during which the wind must be hot. In this case, the peak may be obtained before the RS finishes crossing the shell. Therefore, the decay after the peak is expected to be shallower than the generic value of -2 (even for several orders of magnitude in time), becoming gradually steeper until the generic value is obtained.[10] The second caveat is a highly irregular density profile. Such a profile may result from a highly irregular ejection process in the source, as expected in the internal shock scenario when a burst is highly variable. Since a hydrodynamic evolution smoothes the pressure and the velocity profiles, but not the density profile, such irregularities are expected to be carried by the flow also to the RS phase. If these irregularities in the density profile are large enough, they are expected to be reflected in the RS optical light curve during its rising phase and before its decay reaches the asymptotical value. Thus, a detailed observation of this phase may reveal the exact profile of the ejecta, and may even be used to test the internal shock model (as the density profile in the flow is expected to reflect the light curve produced by internal shocks). Practically, if the early afterglow light curve is highly irregular, with no underlying power law, then the analysis method described here is not applicable, and a theory that describes a highly inhomogeneous RS is required. Note, however, that if the asymptotic value of the decay is reached soon after the peak, the tests of the RS emission (equations 3 and 9) are still applicable.

5 CONCLUSIONS

We have suggested here a parametrization of the early optical emission, as a broken power law with five parameters. We have calculated the values of these parameters for an RS produced by the interaction of baryonic wind with a circumburst ISM. Our main conclusions are as follows.

(i) The optical decay ($\alpha_2 \approx -2$) and the consistency between the peak time and flux of the optical and the radio (equation 8) are robust features of an RS emission in an ISM environment over a large range of initial parameters. Observations of an early optical emission with these features would suggest that:

(i) a significant fraction of outflow energy is baryonic;[11]
(ii) the circumburst medium is ISM-like;
(iii) the RS emission is dominant over other possible sources of optical flash.

(ii) The values of the observables before the optical peak depend strongly on the strength of the shock, ξ, and can be used to pin down the initial conditions of the flow.

(iii) The combination of optical flash and radio flare may also constrain the microscopic parameters in the emitting region.

In addition to the specific optical predictions, we have presented detailed analytical results of the expected emission over the whole spectrum. The advantages of these calculations over previous ones are that they do not make any approximation on the strength of the RS (i.e. relativistic or Newtonian), and that they are confirmed (and corrected) by numerical simulations. The conclusions of these calculations are as follows.

(i) Previous calculations overestimated the intensity of the optical flash. Most pronounced is the Newtonian approximation for $\xi \approx 1$ that overestimates the optical flash by up to three orders of magnitude.

(ii) An optical flash brighter than 15 mag is expected in some but not in all GRBs. A GRB with typical parameters and moderate energy ($E_{52} = 1$) is expected to produce a maximal flux of $R_{\rm mag} \sim$ 17–19 when the RS is mildly relativistic ($\xi \approx 1$).

(iii) Over some reasonable range of the parameter space, the FS emission dominates at all times.

[8] We neglect the feedback of the radiation energy losses on the hydrodynamics. This is justified in the likely case that $\epsilon_{\rm e} \ll 1$.

[9] Note that with a small value for s (broad peak) α_1 reaches its 'asymptotic' value only far from the peak.

[10] This may explain the shallow early decay of GRB 021004. This scenario is very similar to the continuous refreshed RS introduced by Sari & Mészáros (2000), and suggested by Fox et al. (2003b) to explain GRB 021004. The only difference is that here the slow tail of the flow is produced naturally from the hydrodynamics of the relativistic wind and not by a special source activity.

[11] Clearly a small fraction of the outflow energy as a Poynting flux would not change the results presented here, while a very large fraction of Poynting flux will. The fraction of a Poynting flux energy needed to significantly affect these results is yet unclear.

(iv) When the RS is relativistic ($\xi \ll 1$) most of the emission is released in the optical. When ξ increases, the emission is shifted to lower energy bands but it does not reach the radio, as ν_a in this case is $\sim 10^{12-13}$ Hz.

These results suggest a solution to the 'lack' of optical flashes. Only a fraction of the flashes is expected to be bright enough for detection in the current observations, and in some cases a FS emission is expected to dominate from the beginning.

ACKNOWLEDGMENTS

We thank R. Sari and S. Kobayashi for providing us with their relativistic hydrodynamics code and J. Granot, P. Kumar, R. Mochkovitch, F. Daigne and E. Rossi for helpful discussions. The research was supported by the US–Israel BSF and by EU-RTN: GRBs – Enigma and a Tool. EN is supported by the Horowitz foundation and by a Dan David Prize Scholarship 2003.

REFERENCES

Beloborodov A. M., 2002, ApJ, 565, 808
Beuermann K. et al., 1999, A&A, 352, L26
Chevalier R. A., Li Z. Y., 2000, ApJ, 536, 195
Fan Y., Dai Z., Huang Y., Lu T., 2002, ChJAA, 2, 449
Fox D. W. et al., 2003a, ApJ, 586, L5
Fox D. W. et al., 2003b, Nature, 422, 284
Granot J., Sari R., 2001, A&AS, 34, 575
Granot J., Piran T., Sari R., 1999, ApJ, 527, 236
Klotz A., Atteia J. L., Boer M., 2003, GCN Circ., 1961
Kobayashi S., 2000, ApJ, 545, 807
Kobayashi S., Sari R., 2000, ApJ, 542, 819 (KS00)
Kobayashi S., Zhang B., 2003a, ApJ, 582, L75
Kobayashi S., Zhang B., 2003b, ApJ, 597, 455
Kobayashi S., Mészáros P., Zhang B., 2004, ApJ, 601, L13
Kulkarni S. et al., 1999, ApJ, 522, L97
Kumar P., Panaitescu A., 2003, MNRAS, 346, 905
Mészáros P., Rees M. J., 1997, ApJ, 476, 232
Mészáros P., Rees M. J., 1999, MNRAS, 306, L39
Mészáros P., Ramirez-Ruiz E., Rees M. J., 2001, ApJ, 554, 660
Nakar E., Piran T., 2004, preprint (astro-ph/0405473)
Piran T., Sari R., 1998, in Meegan C., Preece R., Koshut T., eds, Gamma-Ray Bursts, 4th Huntsville Symposium. p. 662
Rykoff E., Smith D., 2002, GCN Circ., 1480
Rykoff E. S. et al., 2004, ApJ, 601, 1013
Sari R., Mészáros P., 2000, ApJ, 535, L33
Sari R., Piran T., 1995, ApJ, 455, L143 (SP95)
Sari R., Piran T., 1999a, ApJ, 520, 641
Sari R., Piran T., 1999b, ApJ, 517, L109
Sari R., Piran T., Narayan R., 1998, ApJ, 497, L17
Soderberg A. M., Ramirez-Ruiz E., 2003a, MNRAS, 345, 854
Soderberg A. M., Ramirez-Ruiz E., 2003b, MNRAS, 330, L24
Thompson C., Madau P., 2000, ApJ, 538, 105
Torii K., 2003a, GCN Circ., 2381
Torii K., 2003b, GCN Circ., 2253
Wang X. Y., Dai Z. G., Lu T., 2000, MNRAS, 319, 1159
Weidong L., Alexei V., Ryan C., Saurabh J., 2003, ApJ, 586, L9
Williams G. G., Park H. S., Porrata R., 1999, GCN Circ., 437
Wu X., Dai Z., Huang Y., Lu T., 2003, MNRAS, 342, 1131
Zhang B., Kobayashi S., Mészáros P., 2003, ApJ, 595, 950

This paper has been typeset from a TEX/LATEX file prepared by the author.